


Article

Efficient Machine Learning Model for Predicting the Stiffness of Circular Footings on Clay Overlying Sand

Chongchong Qi ¹, Jiashuai Zheng ¹, Chuiqian Meng ² and Mengting Wu ^{1,*}¹ School of Resources and Safety Engineering, Central South University, Changsha 410083, China² Faculty of Civil Engineering and Geosciences, Delft University of Technology, 2628 Delft, The Netherlands

* Correspondence: 215512109@csu.edu.cn

Abstract: Assessing the stiffness of circular foundations is the key to evaluating their deformation; thus, it is important for foundation design. The current determination methods for the stiffness coefficient are either time-consuming or inaccurate. In this paper, a novel stiffness prediction model has been proposed, using the decision tree (DT) algorithm optimized by particle size optimization (PSO). The condition of the embedded foundation, the embedded depth ($Z_D/2R$), the thickness of the clay layer beneath the foundation base ($T/2R$), and the ratio of shear stiffness between clay and sand ($G_{\text{sand}}/G_{\text{clay}}$) were used as input variables, while the elastic stiffness coefficients (K_C , K_H , K_M , and K_V) were used as output variables. The optimum DT model has undergone comprehensive validation, and independent model verification using extra simulations. The results illustrate that PSO could promote further increases in the capability of DT modeling in predicting stiffness coefficients. The optimum DT model achieved a good level of performance on stiffness coefficient modeling. (The R for the training set was greater than 0.98 for all of the stiffness coefficients.) The variable importance analysis showed that the $T/2R$ was the most significant variable for all stiffness coefficients, followed by $G_{\text{sand}}/G_{\text{clay}}$. The optimum DT model achieved good predictive performance upon independent verification, with the R being 0.97, 0.99, 0.99, and 0.95 for K_V , K_H , K_M , and K_C , respectively. The proposed reliable and efficient DT-PSO model for stiffness coefficients in layered soil could further promote the safe and efficient utilization of circular foundations.



Citation: Qi, C.; Zheng, J.; Meng, C.; Wu, M. Efficient Machine Learning Model for Predicting the Stiffness of Circular Footings on Clay Overlying Sand. *Appl. Sci.* **2023**, *13*, 2653. <https://doi.org/10.3390/app13042653>

Academic Editors: Chin Leo and Raffaele Zinno

Received: 20 December 2022

Revised: 11 February 2023

Accepted: 15 February 2023

Published: 18 February 2023



Copyright: © 2023 by the authors. Licensee MDPI, Basel, Switzerland. This article is an open access article distributed under the terms and conditions of the Creative Commons Attribution (CC BY) license (<https://creativecommons.org/licenses/by/4.0/>).

Keywords: elastic stiffness; circular footing; machine learning; soil–structure interaction

1. Introduction

Circular foundations have been used widely to support onshore and offshore infrastructures, such as transmission towers, oil-drilling platforms, pipeline end manifolds and terminations, and offshore wind turbines [1]. These foundations are subjected to complex loads from self-weight, environmental loads, and accidental loads (e.g., wind, wave, current, storm, ship impact, etc.) [1]. Assessing their stiffness under vertical (V), horizontal (H), and rotational (M) loads is key to predicting the deformation of the whole system.

Numerous studies have been conducted to determine the elastic stiffness of the circular foundations at small strains and provide diagrams or explicit equations for foundation design. For example, based on additional numerical studies and simple physical models, an easy-to-understand dynamic stiffness calculation method was proposed by [2]. For offshore foundations subjected to vertical, horizontal, and torque loads, which can be idealized as rigid circular foundations, Ref. [3] derived a set of empirical expressions for the elastic stiffness coefficients using a small strain linear-elastic perfectly plastic three-dimensional finite element program. Ref. [4] used the scaled boundary finite element to evaluate the load-displacement response of a circular foundation subjected to vertical, horizontal, moment, and torsional loads, as well as the cross-coupling between horizontal and moment loading conditions. However, all these existing studies are limited to a specific circular foundation in a uniform soil layer, whereas in the field, foundation floors are

usually layered with sand and clay. The complexity of the problem also makes it difficult to propose a simple equation that can accurately predict the foundation stiffness under different loading and embedding conditions.

Recently, Ref. [5] performed an extensive elastic analysis on circular foundations on clay overlaying sand under general loading (VHM). The influence of the foundation's embedded condition, the thickness of clay layer beneath the foundation base, and the ratio of shear stiffness between the clay and the sand on the foundation elastic stiffness were quantified. Approximate design equations were proposed. However, limited by the intrinsic feature of the explicit equation, the error in the prediction for certain conditions can be greater than 25%. As the prediction of foundation stiffness under general loading is a typical multi-input/output problem, it is difficult to capture the influence of all of the factors with a simple explicit equation. In addition, three-dimensional elastic simulation is time-consuming and requires extensive pre-experience. Therefore, it is meaningful to have an efficient and accurate model for predicting the foundation stiffness, particularly for large projects (e.g., offshore wind farms) where such calculations need to be conducted repeatedly.

The powerful ability of the machine learning (ML) technique in dealing with multi-input/output problems offers us an alternative solution for foundation design. ML technology can directly learn the relationship between the input variables and the output studied and effectively solve complex nonlinear mapping problems. ML technology has been widely used in many fields of geotechnical engineering, such as parameter identification [6], the development of constitutive models [7], the evaluation of soil liquefaction [8], tunneling [9,10], and rock excavation [11,12]. Apart from the accurate prediction of the outputs, the ML technique can also "smartly" select the most relevant inputs for each output and help the researcher to identify the controlling failure mechanism.

In light of the preceding discussion, this study aimed to develop an efficient ML-based model to predict the stiffness of circular footings on clay overlying sand. The decision tree (DT) modeling technique, optimized by particle swarm optimization (PSO), was adopted in this study. DT is one of the most widely used ML algorithms in geotechnics, which is characterized by robust modeling and high interpretability [13]. Regarding the stiffness of circular foundations in layered soil, ref. [5] performed an extensive study and established a database of stiffness coefficients covering a wide range of foundation and soil conditions. Therefore, the simulation results of [5] were used to train and validate the model. After the comprehensive model training and validation based on the above-mentioned database, a series of independent elastic simulations on circular footings were performed to verify the general applicability of the trained model; The results show that using the trained ML model to simulate each new case can be completed within several seconds with a high level of accuracy. A comprehensive model interpretation was also performed to quantify the importance of each input to each output and to reveal the evolution of the controlling mechanism. We found that ML-based model can not only provide an accurate prediction for the problem, but also help to understand the intrinsic correlation and the underlying mechanism.

2. Research Methodology

Figure 1 illustrates the whole methodology of this study, which includes the following main parts: dataset collection and pre-processing, model construction and evaluation, model interpretation and visualization, and independent verification of the model.

2.1. Dataset Collection Based on Numerical Simulation

This study is concerned with circular foundation stiffness under general loading (VHM) on clay overlying sand. Three different embedded conditions were considered, as shown in Figure 2, including a surface foundation, an embedded foundation with a cavity above, and a fully embedded foundation. For a typical foundation, there were four dimensionless elastic stiffness coefficients, including K_c , K_h , K_m , and K_v . A detailed

explanation of the elastic stiffness of a foundation system under general loading can be found in [5].

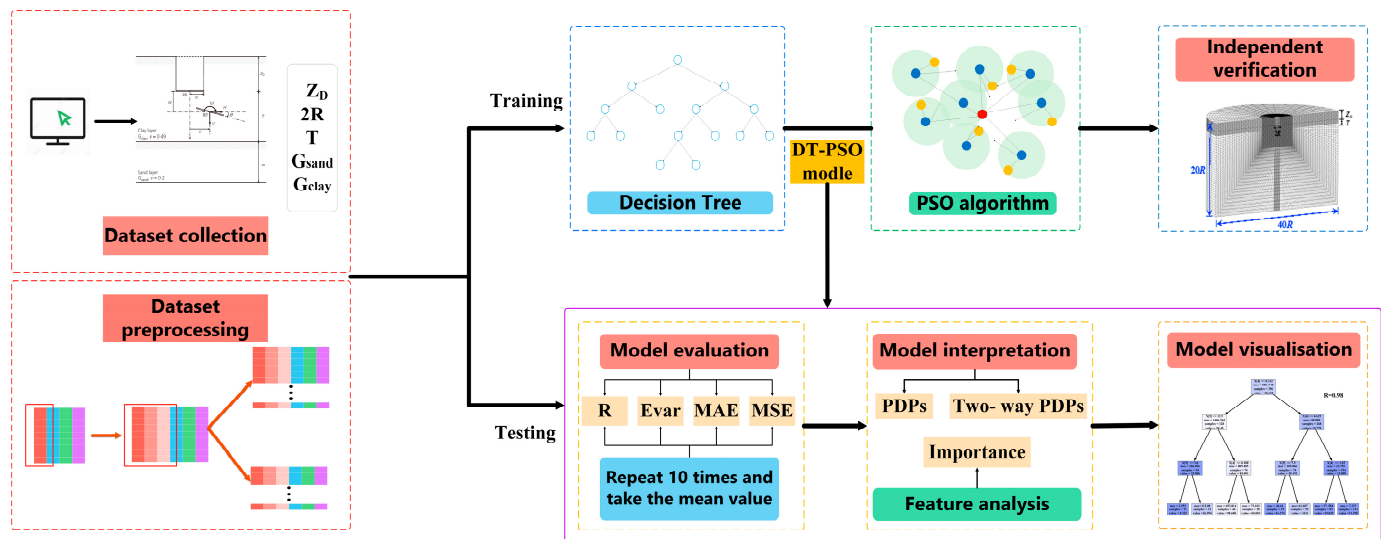


Figure 1. The adopted methodology of this work.

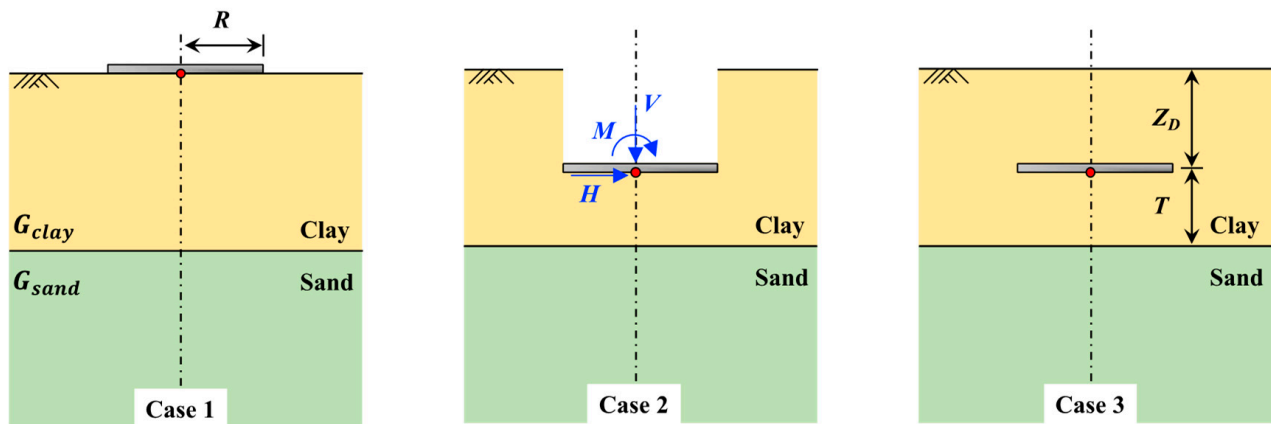


Figure 2. Cases of three embedment conditions.

The dataset used in this study was collected from a series of comprehensive, three-dimensional elastic simulations conducted by [5]. The details of the simulation program are summarized in Table 1. During the numerical simulation, the base was fixed in respect to all three translational directions, while vertical boundaries were fixed in the lateral directions and were free to move vertically. The distance between the footing base and the sand layer ($T/2R$), the stiffness ratio between the sand and the clay (G_{sand}/G_{clay}), the embedment condition (surface, embedded with cavity above, and fully embedded), and the embedment depth ratio ($Z_D/2R$) were selected as inputs, while the dimensionless elastic stiffness coefficients, including K_c , K_h , K_m , and K_v , were the outputs of the training model. Different from other variables, the embedment condition is categorical data, which needs to be transformed into numerical data. In this study, the transformation from categorical data to numerical data was performed using the one-hot encoding [14,15]. After the transformation, the embedment condition was represented by three independent variables, namely case 1 to case 3.

Thus, the final dataset used for modeling consisted of 6 input variables and 4 output variables, for a total of 567 samples. That was, 81 input and output combinations for case 1, and 243 input and output combinations for cases 2 and 3, respectively.

Table 1. The simulation programs in [5] and this study.

	Embedded Condition	Embedded Depth, $Z_D/2R$	Distance to the Sand Layer, $T/2R$	The Ratio of Shear Stiffness, G_{sand}/G_{clay}
model training	Case 1	0	0, 0.125, 0.25, 0.375, 0.5, 0.75, 1, 1.5, 2, 3, ∞	1, 5, 10, 15, 20, 25, 30, 35
	Case 2	0.5, 1, 2	0, 0.125, 0.25, 0.375, 0.5, 0.75, 1, 1.5, 2, 3, ∞	1, 5, 10, 15, 20, 25, 30, 35
	Case 3	0.5, 1, 2	0, 0.125, 0.25, 0.375, 0.5, 0.75, 1, 1.5, 2, 3, ∞	1, 5, 10, 15, 20, 25, 30, 35
This study: numerical model validation	Case 1	0	0, ∞	1
	Case 1	0	0.5	5
This study: training model evaluation	Case 1	0	2.5, 5	5, 10, 20, 40
	Case 2	1.5	2.5, 5	5, 10, 20, 40
	Case 3	1.5	2.5, 5	5, 10, 20, 40

2.2. Dataset Pre-Processing

To speed up the model training and enable the predictive performance comparable, the dataset needs to be standardized. In this paper, the Z-score standardization method was employed (Figure S1). In this method, the original data is standardized as follows:

$$x^* = \frac{x - \mu}{\sigma} \tag{1}$$

where μ is the mean of all sample data, σ is the standard deviation of all sample data, x is the data before normalization, and x^* is the normalized data used for model training.

Figure 3 illustrates the data distribution of inputs and outputs after standardization. Noted that the embedment condition after preprocessing was not shown since a one-hot encoding was employed. The average values of the input variables differ little, but the distribution varied greatly. The distribution of G_{sand}/G_{clay} between 0 and 1 was relatively uniform, but $T/2R$ was mainly concentrated in 0–0.25. Similarly, the average values of K_c , K_h , and K_m outputs were around 0.2, and the distribution was also concentrated between 0 and 0.3. However, the average value of K_v was about 0.5, and the data distribution range was 0.2–0.7.

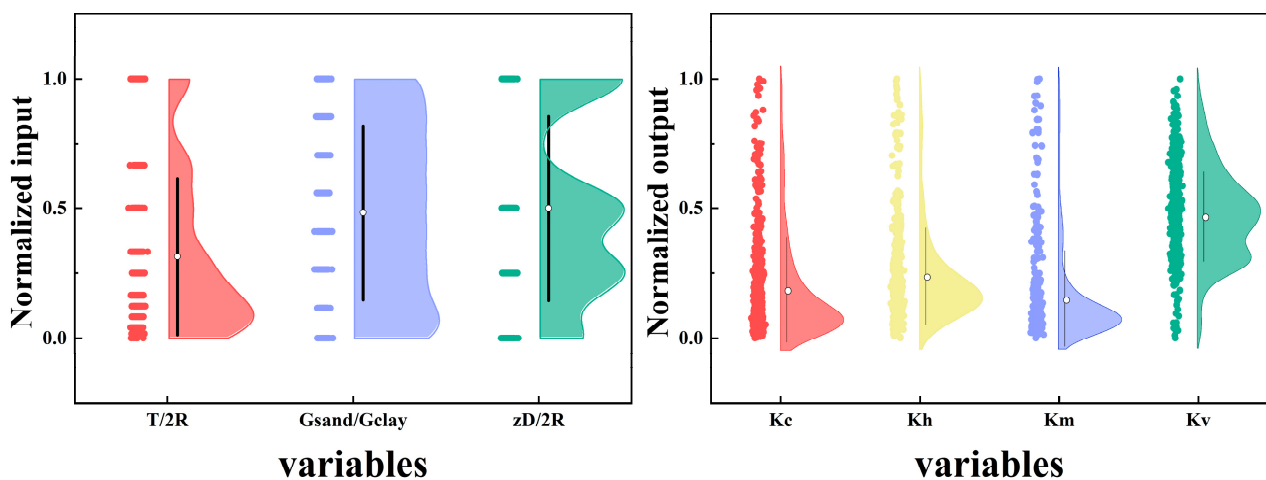


Figure 3. Data distribution of inputs and outputs.

2.3. Machine Learning Modeling

Before constructing the model, the dataset needs to be divided into a training set and a testing set. Among them, the training set is used to train the model, i.e., to learn the relationship between the inputs and the output. The testing set is treated as the independent “new” data to evaluate the generalization capability of the trained ML model [16]. In this study, we used a random split to divide 70% of the data into a training set, and the remaining 30% was used as a testing set [17]. DT and PSO were used to construct a hybrid model. Notably, the random splitting was repeated 10 times, and the average result was regarded as the representative performance during comparison.

The DT is a graphical method of intuitive use of probability analysis that has been widely used for regression and classification problems [18]. The DT technique employs a tree structure to support the decision-making process. In DT, each internal node represents a test on an attribute, each branch represents a test output, and each leaf node represents a category. The decision rules are updated during the DT training process to minimize the discrepancy between the actual and estimated outputs, such as the mean squared error (MSE) for regression problems and the Gini index for classification problems [19]. For the prediction of each new data instance, the model will start with the root node and move downward until reaching the leaf node. The output of the leaf node will be the prediction for this data instance. The DT has been used widely in geotechnical engineering for its flexibility and interpretability [20]. Figure 4 shows a typical DT structure.

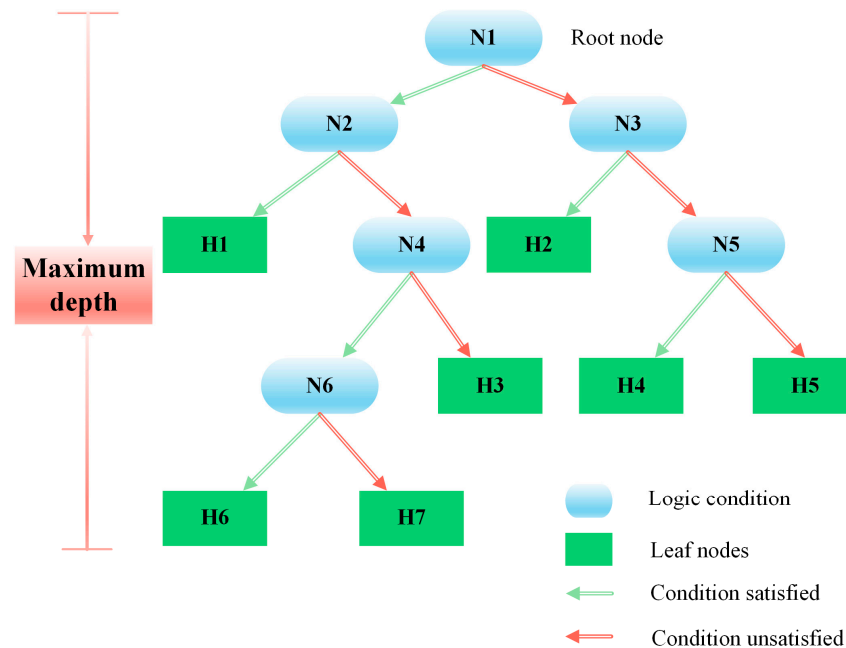


Figure 4. A typical DT structure.

The PSO is a population-based optimization algorithm proposed by [21]. PSO has been widely used in geotechnical engineering due to its simple operation, easy implementation, and rapid convergence to the optimal solution.

PSO imitates the swarm behavior of insects, birds, fish, etc., when they are cooperatively searching for food. Each member of the group is constantly changing its search mode by learning from its own experience and the experience of other members [22]. The solution space is efficiently searched by a particle swarm or population. The first population of particles or individuals is initialized randomly in the solution space. Specifically, the velocity v_i and position x_i of each particle is randomly initialized [23]. The selected fitness function is used to evaluate the performance of each particle, and then the v_i and x_i of

each particle will be updated. After multiple generations, the optimal solution is obtained (Figure 5). The update strategy is shown as follows:

$$v_i^{t+1} = w \times v_i^t + c_1 \times r_1(p_{best,i}^t - x_i^t) + c_2 \times r_2(g_{best}^t - x_i^t) \tag{2}$$

$$x_i^{t+1} = x_i^t + v_i^{t+1} \tag{3}$$

where v_i^t and v_i^{t+1} represent the velocity of the i individual at t -th and $(t + 1)$ -th generation, respectively; x_i^t and x_i^{t+1} represent positions of i -th individual; w , c_1 , and c_2 are the inertia parameter, the cognitive influence parameter, and the social influence parameter, respectively; r_1 and r_2 are random values between 0 and 1; $p_{best,i}^t$ and g_{best}^t represent the best position of an individual and the group's best position at t -th generation.

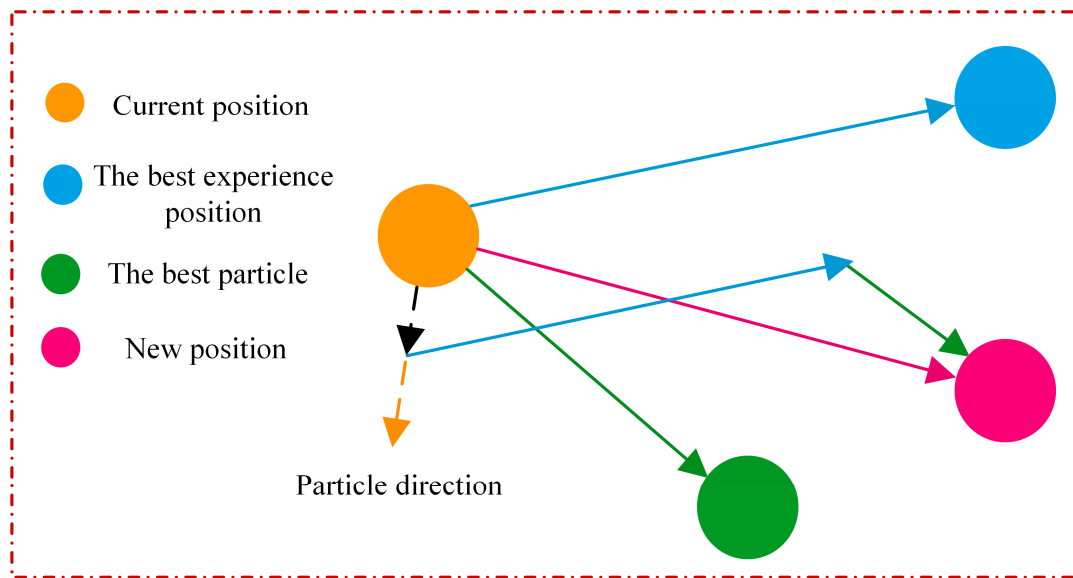


Figure 5. Schematic diagram of the PSO method.

The performance of the DT model on a specific dataset is controlled by hyper-parameters. Thus, we used PSO to tune the hyper-parameters of the DT model. Table 2 summarizes the PSO parameters employed in this study [24,25].

Table 2. PSO parameters employed in this work.

Parameters	Settings	Parameters	Settings
Fitness function	The cross-validation performance (R)	Population size	200
Maximum generation	50	w	$(1 + \text{random})/2$
c_1	1.8	c_2	1.8

Note: “random” represents a random value between 0 and 1.

Based on the suggestions and preliminary tests in the literature [26–28], the hyper-parameters that needed to be tuned and their ranges were determined: the maximum depth limited by the DT when building subtrees (max_depth: 3–15), the minimum number of samples required for the splitting of an internal node (min_samples_split: 2–15), the minimum number of samples included in the leaf node (min_samples_leaf: 1–15), and the maximum percentage of variables considered during splitting (max_features: 0.4–1.0).

K -fold cross-validation (CV) was employed for the evaluation of the training performance. In k -fold CV, the training set is further divided into k -folds. Model training is performed using $(k-1)$ folds and the remaining fold is used for validation [29]. The training-validation process is repeated k times, such that the whole training set is predicted. The

average performance derived from the k -fold CV is taken as the training performance of the model. Considering the convergence and computational time, k was set as 5 in this study.

2.4. Performance Evaluation

In this paper, correlation coefficient (R), explained variance score (Evar), mean absolute error (MAE) and mean squared error (MSE) were selected as evaluate indicators of predictive performance [30], which can be calculated as follows:

$$R = \frac{\sum_{i=1}^N (y_i^* - \bar{y}^*)(y_i - \bar{y})}{\sqrt{\sum_{i=1}^N (y_i^* - \bar{y}^*)^2} \sqrt{\sum_{i=1}^N (y_i - \bar{y})^2}} \quad (4)$$

$$\text{Evar} = 1 - \frac{\text{Var}\{y_i - y_i^*\}}{\text{Var}\{y_i\}} \quad (5)$$

$$\text{MAE} = \frac{1}{N} \sum_{i=1}^N |y_i - y_i^*| \quad (6)$$

$$\text{MSE} = \frac{1}{N} \sum_{i=1}^N (y_i - y_i^*)^2 \quad (7)$$

where N is the number of samples; y_i and y_i^* are the actual and estimated value of the i -th instance; \bar{y} and \bar{y}^* are the average values of the actual and estimated outputs; and Var represents the variance.

2.5. Model Interpretation

To promote ML-aided knowledge discovery, various methods were employed to interpret the ML models. In this study, two different methods, including variable importance score and partial dependence plots (PDPs) [31], were adopted.

- Variable importance score

Variable importance is scored according to how useful the input variables are to predicting the target variable [32]. There are many types and calculation methods of variable importance. For the DT algorithm, the importance score is obtained based on the reduction of the Gini coefficient or entropy, which can be achieved with the `feature_importances_` attribute in scikit-learn.

- Partial dependence plots (PDPs)

Unlike variable importance, which assigns a score for each variable, partial dependence plots (PDPs) show how variables affect model predictions. More specifically, PDPs not only reflect the significance of each input variable to the output, but they also indicate how that input variable will influence the output, i.e., negatively or positively [33]. PDPs can highlight the marginal effect of one or two variables on the prediction results of ML models. Due to the non-parametric characteristics of many ML algorithms, PDPs can reveal linear and nonlinear variables, making them easy to understand with high explanatory power [34].

2.6. Independent Model Verification

In addition to the database in [5], extra simulations were also performed in this study to provide an independent evaluation dataset. All the simulations were performed using the FE software Abaqus 6.14 [35]. The FE mesh in Figure 6 (Case 2, $Z_D/2R = 1.5$, $T/2R = 0.5$) is typical of the meshes employed in all analyses. Considering the symmetry of the problem, only half of the pile–soil system was modeled. Just as in [5], the footing has a radius of R and a thickness of $R/50$. The soil domain was chosen as $200R$ (R is the radius of the

foundation) in diameter and $200R$ in depth. Both the soil and foundation were simulated with eight-node linear strain brick elements (i.e., ‘C3D8’). A sensitivity analysis with the model doubling the mesh density and geometric dimensions showed a difference of less than 3% of the stiffness coefficients. The interface behavior between the pile and soil was assumed to be fully rough and modeled using the “tie” constraint in Abaqus. The soil was modeled by an elastic model, which is fully characterized by two parameters: the shear modulus and Poisson’s ratio. In this study, Poisson’s ratio was assumed to be constant values of 0.2 and 0.49 for sand and clay, respectively, while the ratio of shear stiffness between clay and sand ($G_{\text{sand}}/G_{\text{clay}}$) varied from 1 to 40. In the end, a total of 108 extra elastic simulations were performed in this study, with 12 of them dedicated to numerical model validation and the other 96 cases dedicated to the independent evaluation of the trained model. Details about the simulations conducted in this study can be found in Table 1.

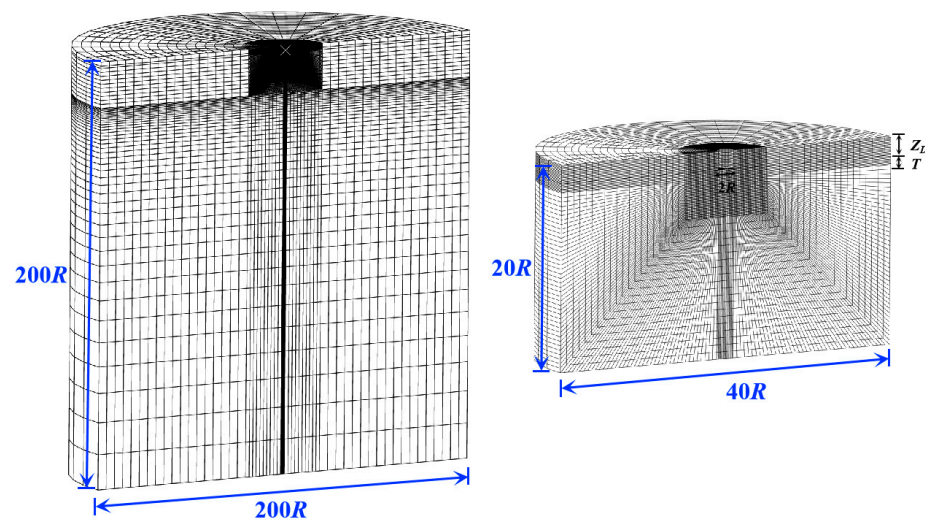


Figure 6. Typical FEM mesh employed in this study.

Table 3 shows the comparison of the elastic stiffness coefficients between the computed values using the numerical model in this study and those from [5]. All the FE simulations were performed on a computer, the CPU and RAM of which were Intel (R) Xeon (R) W-2223 CPU @ 3.60 GHz and 16 GB, respectively. In total, it required more than 100 h to finish all the simulations. As shown in the table, for all 12 simulation cases, the numerical model in this study can predict the elastic stiffness coefficients of the foundation under various loading conditions well. The maximum difference between this study and [5] is less than 1%.

Table 3. Comparison of the elastic coefficients between this study and [5].

NO.	Embedded Condition	$Z_D/2R$	$T/2R$	$G_{\text{sand}}/G_{\text{clay}}$	K_V	K_H	K_M	K_C
1	Case 1	0	0	1	5.273 (0.04%)	4.578 (0.15%)	3.634 (0.80%)	−0.567 (0.60%)
2	Case 1	0	0.5	5	16.963 (0.30%)	7.030 (0.35%)	6.623 (0.8%)	0.408 (0.75%)
3	Case 1	0	∞	1	7.954 (0.14%)	5.353 (0.24%)	5.217 (0.60%)	−0.030 (1.00%)

Note: the value in the bracket represents the percentage of the difference between this study and [5].

3. Results and Discussion

3.1. Hyper-Parameters Tuning

To improve model performance, regression indicator R was used as the objective function of PSO optimization to tune the hyper-parameters. The hyper-parameters of the models with K_c , K_h , K_m , and K_v as target variables were tuned 5 times, and the average performance R represented by the solid line was the final performance of the model. As shown in Figure 7, the CV training performance gradually improved with the iteration of PSO, and it was mainly realized in the first 10 iterations. Taking the K_c dataset as an example, the average R-value increased from 0.982 to 0.987 after hyper-parameter tuning and then remained unchanged, demonstrating the efficiency of PSO in fine-tuning the DT's hyper-parameters.

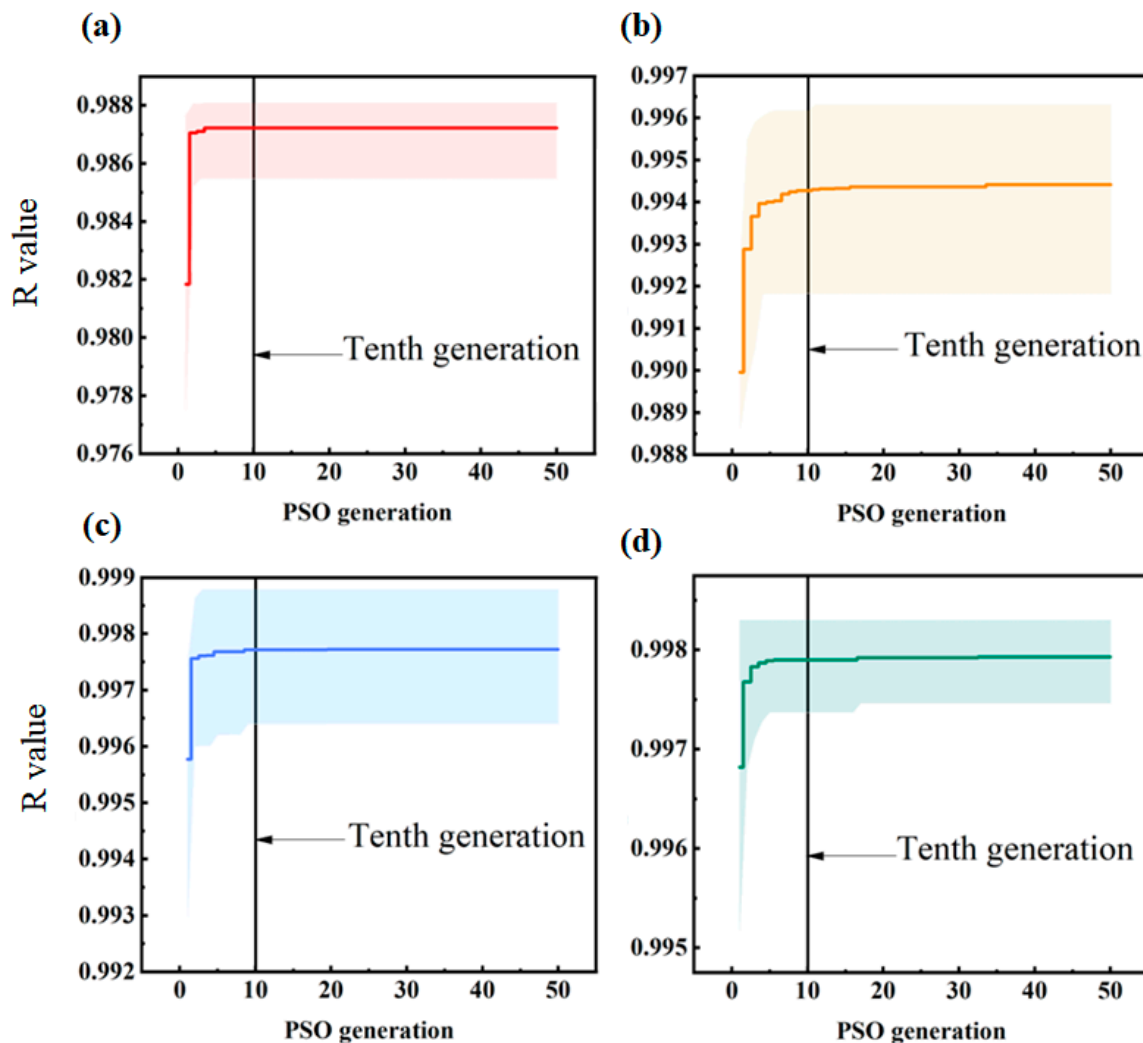


Figure 7. The change of CV training performance R with PSO iterations on datasets (a) K_c , (b) K_h , (c) K_m , and (d) K_v . Each generation took about 2 h to calculate.

Table 4 summarizes the optimal hyper-parameters for four datasets. As shown, the optimal `max_depth` is in the range of 10 to 14, depending on the dataset. The `min_samples_split` was determined to be 3 for K_c , while a constant value of 2 was determined for the remaining three datasets. For the other two hyper-parameters, the same optimal values were used for all datasets. Consistent with observations in a previous study [36], the optimized results suggest that the performance of a typical DT model is mainly controlled by the `max_depth` and is relatively insensitive to other hyper-parameters.

Table 4. The optimal DT hyper-parameters after PSO tuning.

Hyper-Parameters	K_c	K_h	K_m	K_v
max_depth	10	13	12	14
min_samples_split	3	2	2	2
Other hyper-parameters	min_samples_leaf = 1, max_features = 1			

3.2. Model Evaluation and Visualization

Figure 8 shows the model’s performance after tuning the hyper-parameters on the datasets with K_c , K_h , K_m , and K_v as target variables, respectively. The R and Evar values of both the training and testing sets were higher than 0.9, and the MSE and MAE maintained low values. In addition, the R values on four datasets were all higher than those before hyper-parameter tuning (Figure S1). The above analysis not only showed that the PSO-DT model had excellent prediction and generalization ability, but it also confirmed the role of PSO tuning [37,38].

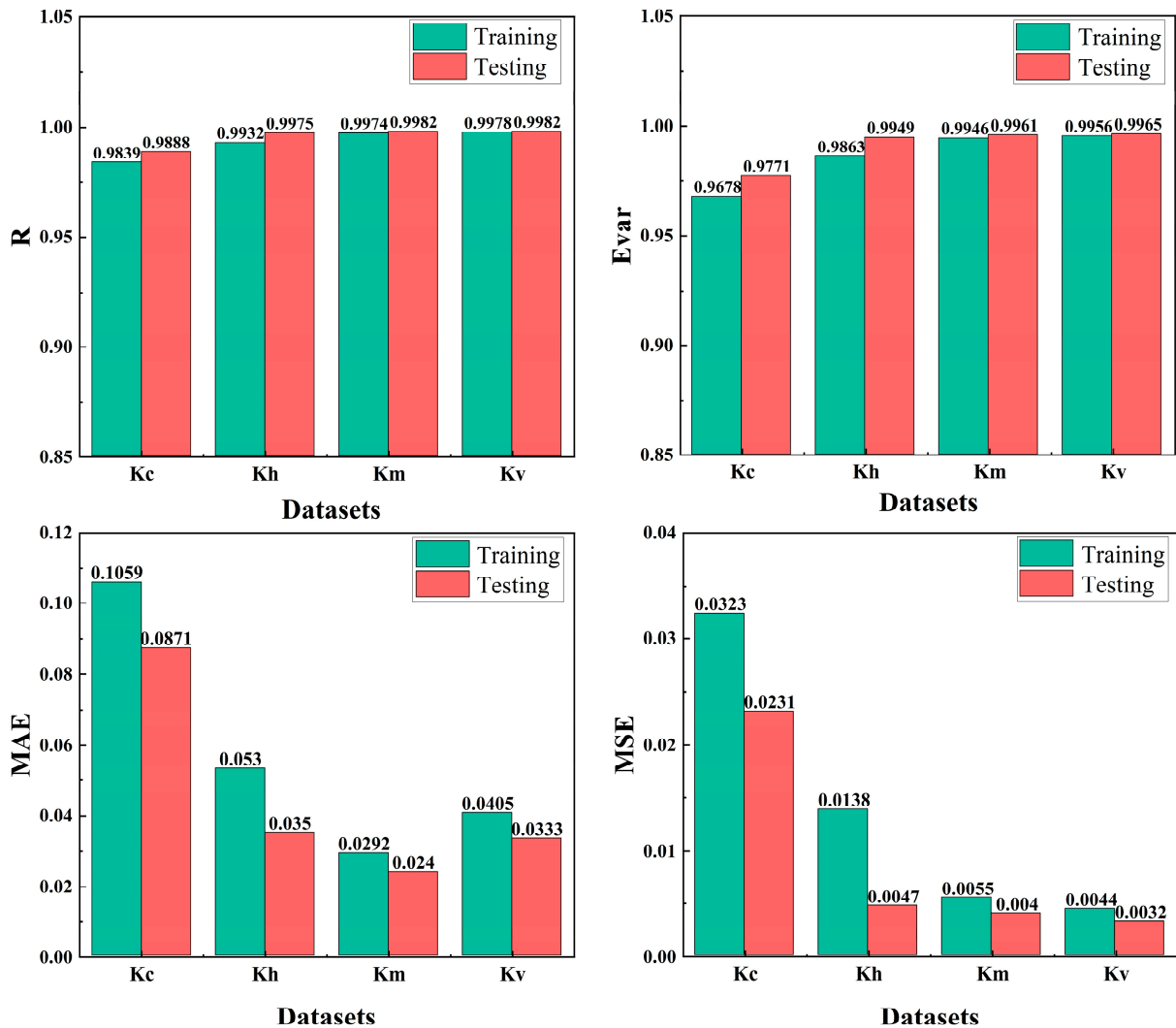


Figure 8. Performance evaluation of the DT-PSO model on four datasets.

Figure 9 presents a visual comparison of the actual and estimated dimensionless elastic stiffness coefficients. The diagonal line in the figure represents the best prediction curve, where the estimated output equals the actual output. As illustrated, the points were distributed close to the diagonal line, indicating that an excellent prediction was achieved.

The MSE values of the training and testing sets were small (less than 0.05), and the R-square (R^2) was higher than 0.99, which further confirmed the accuracy of the prediction.

Figure 10 presents a visualization of a DT for the K_c dataset. To maintain the interpretation of the DT, the max_depth was restrained to 4 as an example. It should be noted that good predictive performance (CV training performance = 0.96) was also achieved under this condition. The decision rule, MSE value, the number of samples, and the mean value can be identified in Figure 10. Only $T/2R$ and G_{sand}/G_{clay} were employed during the construction of the decision rules, implying the significance of these two input variables. The variable importance will be further discussed in the following section.

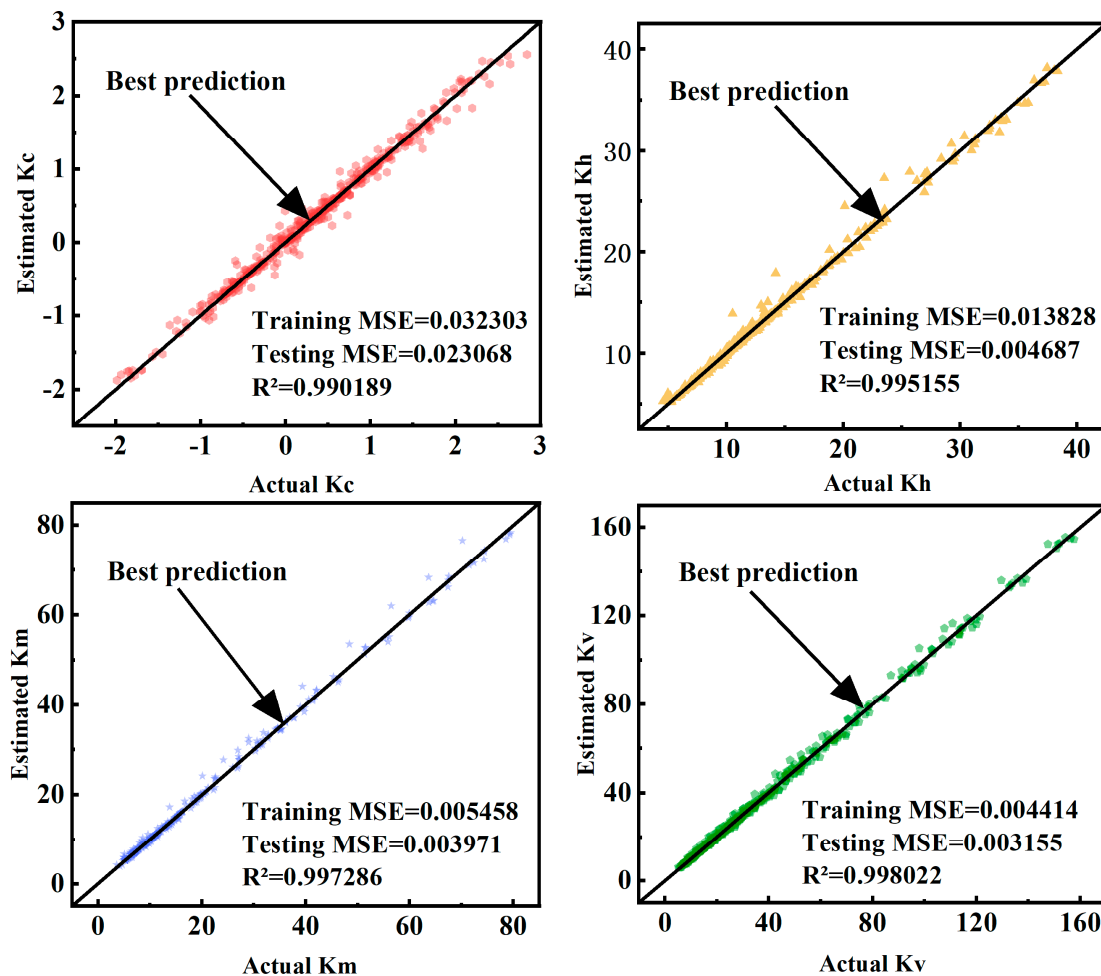


Figure 9. Scatter plot of the actual and predicted dimensionless elastic stiffness coefficients.

3.3. Model Interpretation

Figure 11 shows the variable importance score for different inputs for the four datasets. As illustrated, $T/2R$ was the most significant variable for all stiffness coefficients, with an average variable importance score of around 0.58. This suggested that soil layering played an important role in foundation stiffness. Furthermore, it can be seen that the importance of the $T/2R$ on the four stiffness coefficients was comparable, which means that the soil layering affected the foundation's kinematic behavior under all loading conditions. The G_{sand}/G_{clay} also contributed greatly to the output, and its average variable importance score was 0.30. Unlike the nearly equal influence of $T/2R$ on all stiffness coefficients, the importance of G_{sand}/G_{clay} was most significant for the vertical foundation stiffness coefficient. The above results were in good agreement with the DT visualization results in Figure 10. Comparatively speaking, the influence of other input variables on output variables was relatively small, but it cannot be ignored. For example, embedment conditions

had an obvious influence on the kinematic behavior of circular foundations under lateral load, and the importance of Case 2 reached 0.2388.

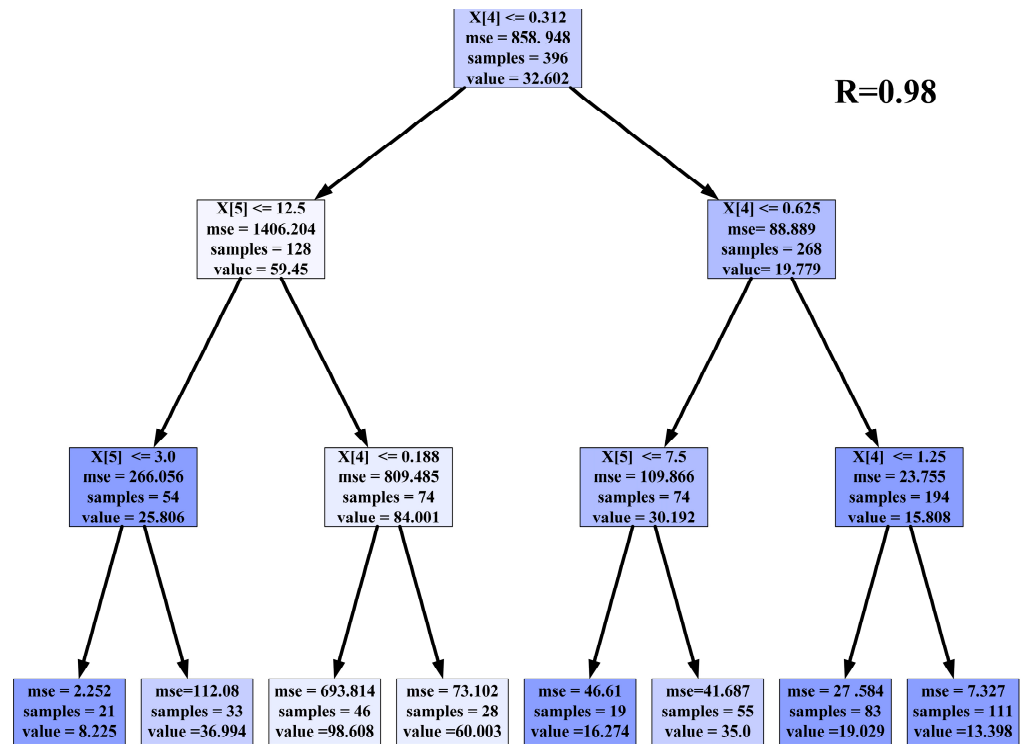


Figure 10. The visualization of a DT for K_c . Note that $X[4]$ and $X[5]$ represent $T/2R$ and G_{sand}/G_{clay} , respectively.

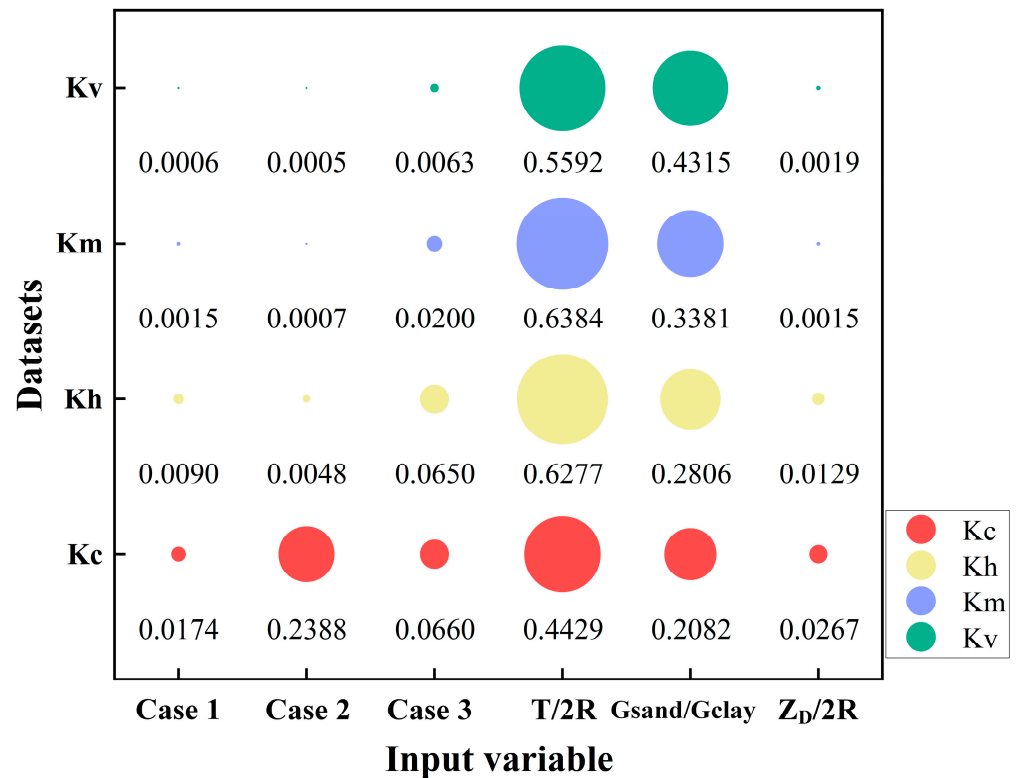


Figure 11. Variable importance score for four datasets.

Figure 12 analyzes how the features $T/2R$, G_{sand}/G_{clay} , and $Z_D/2R$ affected the prediction for the target variables K_c , K_h , K_m , and K_v . $T/2R$ had the greatest influence on the stiffness coefficient and was negatively correlated with K_h , K_m , and K_v . Within a certain $T/2R$ range (normalized $T/2R < 0.2$), the values of K_h , K_m , and K_v decreased rapidly with the increase in $T/2R$. When the value of $T/2R$ was greater than 0.2, K_h , K_m , and K_v tended to remain unchanged. While K_c first increased and then decreased with the increase in the $T/2R$ value, 0.1 was the critical value of K_c change. Furthermore, we also found that G_{sand}/G_{clay} was positively correlated with K_c , K_h , K_m , and K_v ; with the gradual increase in the feature value of $Z_D/2R$, K_c , K_h , K_m , and K_v changed little, indicating that $Z_D/2R$ was relatively less important for the stiffness coefficient.

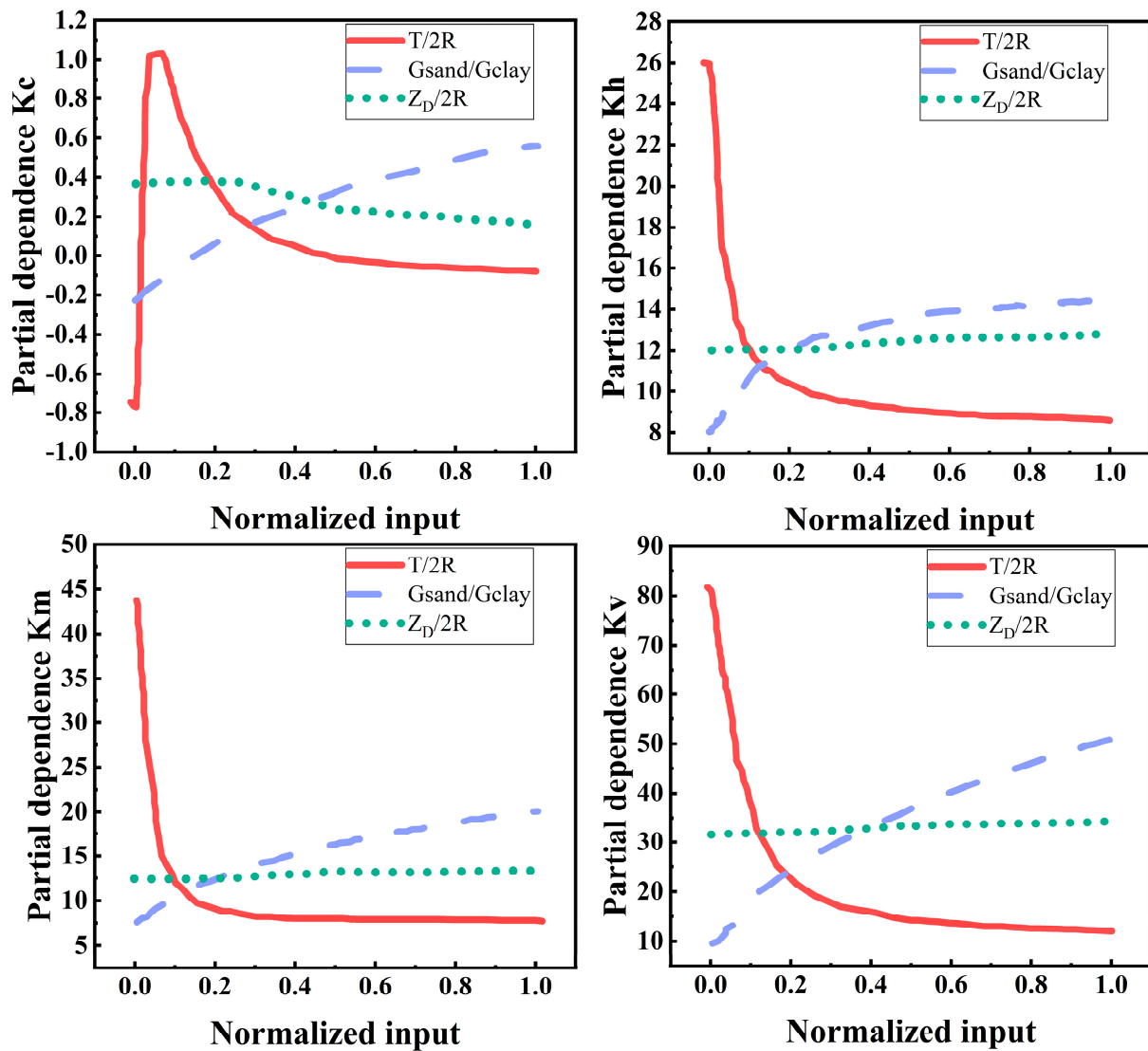


Figure 12. PDPs of $T/2R$, G_{sand}/G_{clay} , and $Z_D/2R$ for all output variables. Note that the features were normalized so that their influences on the output could be better compared.

Figure 13 further illustrates the interaction influence of input variables on the output, taking the K_c dataset as an example. There is a strong correlation among $T/2R$, G_{sand}/G_{clay} , and $Z_D/2R$, and they affect the stiffness coefficient in a coupled way. For example, when $T/2R$ was less than 0.25 and G_{sand}/G_{clay} was more than 20, the model tended to predict a large K_c . A large K_c was also observed when G_{sand}/G_{clay} was greater than 30 and the $Z_D/2R$ was in the range of 0–0.5. The above analysis provided a certain reference for improving the stiffness of the circular foundation.

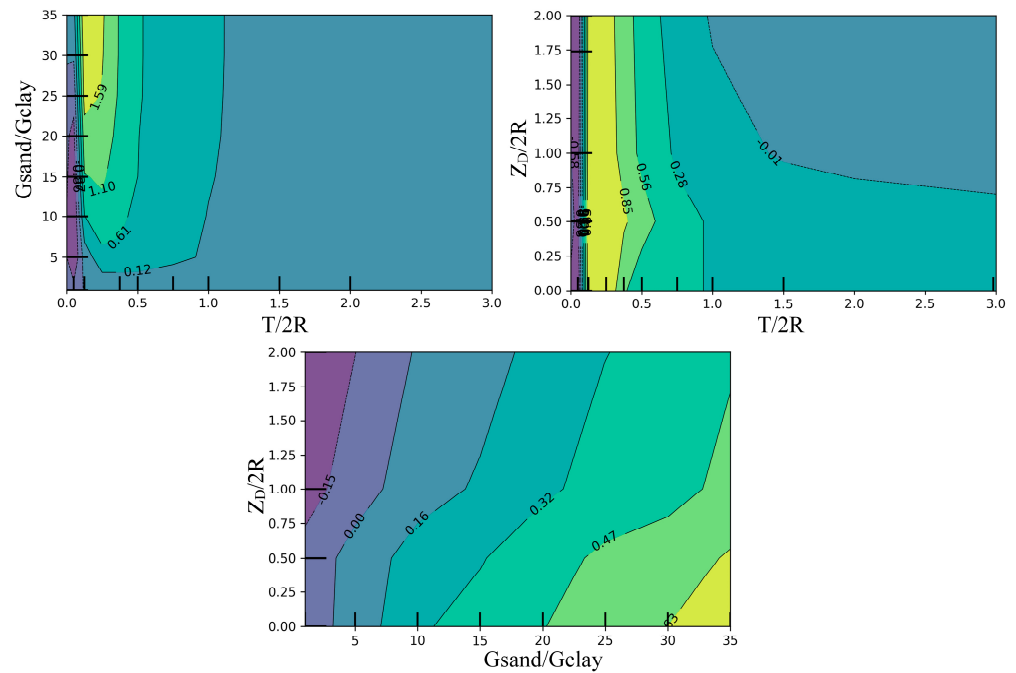


Figure 13. PDP interaction of $T/2R$, G_{sand}/G_{clay} , and $Z_D/2R$ on the K_c dataset.

3.4. Independent Model Verification

In the preceding section, it was demonstrated that the DT-based ML model can provide an accurate prediction of the foundation stiffness in layered soil and revealed the relationship between the input variables and the stiffness coefficients. To further demonstrate the general accuracy of the trained model, we utilized the DT-PSO model to predict the basic stiffness for an additional 96 independent validation cases.

As shown in Figure 14a, for K_v , K_h , K_m , and K_c , the R values between the true and predicted values reached 0.97, 0.99, 0.99, and 0.95, respectively, indicating that the model performance is pretty good. The differences between the four true and predicted foundation stiffness coefficients are all within the acceptable error range (Figure 14b). More importantly, it should be noted that the DT model was run on a personal computer with the CPU and RAM of an Intel (R) Xeon (R) W-2223 CPU @ 3.60 GHz and 16 GB. For all the validation cases, the prediction using the DT model took less than 1 s. We are therefore confident in saying that the DT model is reliable and efficient in predicting the foundation stiffness in layered soil and can be used in foundation design.

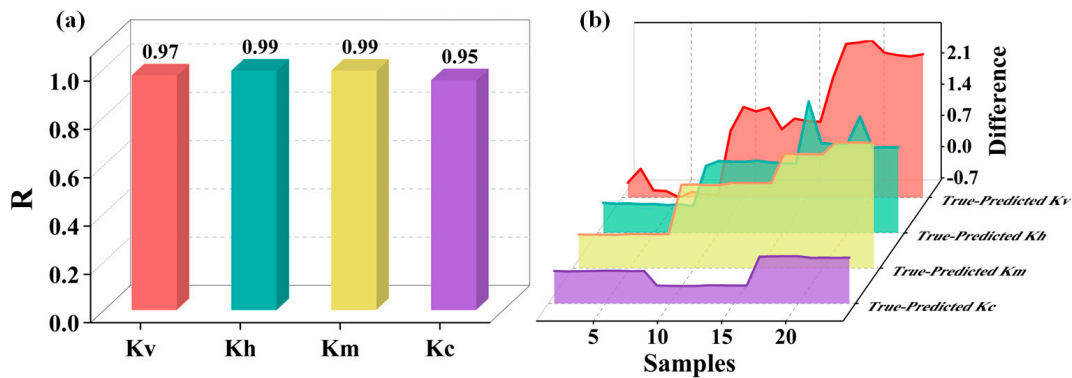


Figure 14. Independent verification of model feasibility: (a) Evaluation of four foundation stiffness coefficient models using R; (b) Consistency of foundation stiffness calculated by FE model and DT model.

4. Conclusions

The stiffness coefficient is an important parameter to be considered in designing circular foundations. The current determination methods for the stiffness coefficient were either time-consuming or inaccurate. In this study, three-dimensional elastic simulation data were collected via a literature search to construct a hybrid model PSO-DT to predict the stiffness coefficient quickly and accurately. Extra finite-element simulation data were used for independent validation of the model. Furthermore, variable importance and PDP were used to analyze the sensitivity of different features. The specific conclusions were as follow:

1. For K_v , K_h , K_m , and K_c , the R and Evar value of the DT model, as tuned by PSO on the training and testing sets, were both higher than 0.95, and the MSE and MAE were less than 0.15, indicating that the model had a high level of robustness.
2. Feature importance showed that $T/2R$ had the most significant effect on the four stiffness coefficients, with an average importance value of about 0.58. Furthermore, there were differences in the way features affected output variables. When a $T/2R$ less than 0.5 interacted with $G_{\text{sand}}/G_{\text{clay}}$ and $Z_D/2R$ in a coupled way, the effect on the stiffness coefficient was greater.
3. Independent verification results showed that the R values between the true and predicted stiffness coefficients (K_v , K_h , K_m , and K_c) were 0.97, 0.99, 0.99, and 0.95, respectively, indicating that the model has a high level of generalization.

In the future, many other variables should be considered in ML modeling, such as the water table, the difference in the soil profile, etc. Moreover, other important parameters for foundation design, such as the lower and upper bounds of plasticity, should be included. Finally, other advanced ML algorithms should be used, and more advanced feature engineering and data pre-processing techniques should be attempted.

Supplementary Materials: The following supporting information can be downloaded at: <https://www.mdpi.com/article/10.3390/app13042653/s1>, Figure S1: Performance of model using DT default parameters on (a) original and (b) normalized datasets.

Author Contributions: Conceptualization, C.Q. and M.W.; methodology, C.Q. and J.Z.; software, M.W.; validation, C.Q. and C.M.; formal analysis, C.M.; investigation, J.Z.; resources, C.Q.; data curation, C.M.; writing—original draft preparation, C.Q. and J.Z.; writing—review and editing, C.Q. and M.W.; visualization, J.Z.; supervision, C.Q.; project administration, C.M.; funding acquisition, C.Q. All authors have read and agreed to the published version of the manuscript.

Funding: This work was supported by the State Key Laboratory of Hydraulic Engineering Simulation and Safety, Tianjin University (No. HESS-2120).

Data Availability Statement: The data presented in this study are available upon request from the corresponding author.

Conflicts of Interest: The authors declare no conflict of interest.

References

1. Randolph, M.; Gourvenec, S. *Offshore Geotechnical Engineering*; CRC Press: Boca Raton, FL, USA, 2017.
2. Dobry, R.; Gazetas, G. Dynamic response of arbitrarily shaped foundations. *J. Geotech. Engng.* **1986**, *112*, 109–135. [[CrossRef](#)]
3. Ngo-Tran, C.L. The Analysis of Offshore Foundations Subjected to Combined Loading. Ph.D. Thesis, University of Oxford, Oxford, UK, 1996.
4. Doherty, J.P.; Deeks, A.J. Elastic response of circular footings embedded in a non-homogeneous half-space. *Géotechnique* **2003**, *53*, 703–714. [[CrossRef](#)]
5. Wang, Y.; Cassidy, M.J.; Bienen, B. Elastic stiffness of circular footings on clay overlying sand under general loading. *Géotechnique Lett.* **2020**, *10*, 498–509. [[CrossRef](#)]
6. Hasanipanah, M.; Jamei, M.; Mohammed, A.S.; Amar, M.N.; Hocine, O.; Khedher, K.M. Intelligent prediction of rock mass deformation modulus through three optimized cascaded forward neural network models. *Earth Sci. Inform.* **2022**, *15*, 1659–1669. [[CrossRef](#)]

7. Guan, Q.; Yang, Z.; Guo, N.; Hu, Z. Finite element geotechnical analysis incorporating deep learning-based soil model. *Comput. Geotech.* **2023**, *154*, 105120. [[CrossRef](#)]
8. Zhao, Z.; Duan, W.; Cai, G. A novel PSO-KELM based soil liquefaction potential evaluation system using CPT and Vs measurements. *Soil Dyn. Earthq. Eng.* **2021**, *150*, 106930. [[CrossRef](#)]
9. Chen, R.; Zhang, P.; Wu, H.; Wang, Z.; Zhong, Z. Prediction of shield tunneling-induced ground settlement using machine learning techniques. *Front. Struct. Civ. Eng.* **2019**, *13*, 1363–1378. [[CrossRef](#)]
10. Huang, H.; Chang, J.; Zhang, D.; Zhang, J.; Wu, H.; Li, G. Machine learning-based automatic control of tunneling posture of shield machine. *J. Rock Mech. Geotech. Eng.* **2022**, *14*, 1153–1164. [[CrossRef](#)]
11. Hasanipanah, M.; Keshtegar, B.; Thai, D.-K.; Troung, N.-T. An ANN-adaptive dynamical harmony search algorithm to approximate the flyrock resulting from blasting. *Eng. Comput.* **2020**, *38*, 1257–1269. [[CrossRef](#)]
12. Jamei, M.; Hasanipanah, M.; Karbasi, M.; Ahmadianfar, I.; Taherifar, S. Prediction of flyrock induced by mine blasting using a novel kernel-based extreme learning machine. *J. Rock Mech. Geotech. Eng.* **2021**, *13*, 1438–1451. [[CrossRef](#)]
13. Garnica-Caparrós, M.; Memmert, D. Understanding gender differences in professional European football through machine learning interpretability and match actions data. *Sci. Rep.* **2021**, *11*, 10805. [[CrossRef](#)] [[PubMed](#)]
14. Wu, J.; Zhang, Q.; Zhao, Y.; Liu, Y.; Chen, A.; Li, X.; Wu, T.; Li, J.; Guo, Y.; Liu, A. Radiomics analysis of iodine-based material decomposition images with dual-energy computed tomography imaging for preoperatively predicting microsatellite instability status in colorectal cancer. *Front. Oncol.* **2019**, *9*, 1250. [[CrossRef](#)] [[PubMed](#)]
15. Qi, C.; Fourie, A.; Chen, Q.; Tang, X.; Zhang, Q.; Gao, R. Data-driven modelling of the flocculation process on mineral processing tailings treatment. *J. Clean. Prod.* **2018**, *196*, 505–516. [[CrossRef](#)]
16. Wang, Z.; Liu, T.; Long, Z.; Wang, J.; Zhang, J. A machine-learning-based model for predicting the effective stiffness of precast concrete columns. *Eng. Struct.* **2022**, *260*, 114224. [[CrossRef](#)]
17. Zhang, W.; Zhang, R.; Wu, C.; Goh, A.T.; Wang, L. Assessment of basal heave stability for braced excavations in anisotropic clay using extreme gradient boosting and random forest regression. *Undergr. Space* **2020**, *7*, 233–241. [[CrossRef](#)]
18. Kushwah, J.S.; Kumar, A.; Patel, S.; Soni, R.; Gawande, A.; Gupta, S. Comparative study of regressor and classifier with decision tree using modern tools. *Mater. Today Proc.* **2021**, *56*, 3571–3576. [[CrossRef](#)]
19. Chou, J.-S.; Yang, K.-H.; Pampang, J.P.; Pham, A.-D. Evolutionary metaheuristic intelligence to simulate tensile loads in reinforcement for geosynthetic-reinforced soil structures. *Comput. Geotech.* **2015**, *66*, 1–15. [[CrossRef](#)]
20. He, X.; Xu, H.; Sabetamal, H.; Sheng, D. Machine learning aided stochastic reliability analysis of spatially variable slopes. *Comput. Geotech.* **2020**, *126*, 103711. [[CrossRef](#)]
21. Eberhart, R.; Kennedy, J. A new optimizer using particle swarm theory, MHS'95. In Proceedings of the Sixth International Symposium on Micro Machine and Human Science, Nagoya, Japan, 4–6 October 1995; pp. 39–43.
22. Wang, G.; Ma, Z. Hybrid particle swarm optimization for first-order reliability method. *Comput. Geotech.* **2017**, *81*, 49–58. [[CrossRef](#)]
23. Ray, R.; Kumar, D.; Samui, P.; Roy, L.B.; Goh, A.; Zhang, W. Application of soft computing techniques for shallow foundation reliability in geotechnical engineering. *Geosci. Front.* **2020**, *12*, 375–383. [[CrossRef](#)]
24. Eberhart, R.C.; Shi, Y. Tracking and optimizing dynamic systems with particle swarms. In Proceedings of the 2001 Congress on Evolutionary Computation, Seoul, Republic of Korea, 27–30 May 2001; Volume 101, pp. 94–100.
25. Armaghani, D.J.; Hajihassani, M.; Bejarbaneh, B.Y.; Marto, A.; Mohamad, E.T. Indirect measure of shale shear strength parameters by means of rock index tests through an optimized artificial neural network. *Measurement* **2014**, *55*, 487–498. [[CrossRef](#)]
26. Alexey, N.; Alois, K. Gradient boosting machines, a tutorial. *Front. Neurobot.* **2013**, *7*, 21.
27. Breiman, L. Random Forests. *Mach. Learn.* **2001**, *45*, 5–32. [[CrossRef](#)]
28. Qi, C.; Chen, Q.; Fourie, A.; Zhang, Q. An intelligent modelling framework for mechanical properties of cemented paste backfill. *Miner. Eng.* **2018**, *123*, 16–27. [[CrossRef](#)]
29. Xiong, Z.; Cui, Y.; Liu, Z.; Zhao, Y.; Hu, M.; Hu, J. Evaluating explorative prediction power of machine learning algorithms for materials discovery using k-fold forward cross-validation. *Comput. Mater. Sci.* **2020**, *171*, 109203. [[CrossRef](#)]
30. Qi, C.; Wu, M.; Zheng, J.; Chen, Q.; Chai, L. Rapid identification of reactivity for the efficient recycling of coal fly ash: Hybrid machine learning modeling and interpretation. *J. Clean. Prod.* **2022**, *343*, 130958. [[CrossRef](#)]
31. Zhou, J.; Li, E.; Yang, S.; Wang, M.; Shi, X.; Yao, S.; Mitri, H.S. Slope stability prediction for circular mode failure using gradient boosting machine approach based on an updated database of case histories. *Saf. Sci.* **2019**, *118*, 505–518. [[CrossRef](#)]
32. Krzywinski, M.; Altman, N. Classification and regression trees. *Nat. Methods* **2017**, *14*, 757–758. [[CrossRef](#)]
33. Pacifici, M.; Rondinini, C.; Rhodes, J.R.; Burbidge, A.A.; Cristiano, A.; Watson, J.E.M.; Woinarski, J.C.Z.; Di Marco, M. Global correlates of range contractions and expansions in terrestrial mammals. *Nat. Commun.* **2020**, *11*, 2840. [[CrossRef](#)]
34. Mokhtari, S.; Mooney, M.A. Predicting EPBM advance rate performance using support vector regression modeling. *Tunn. Undergr. Space Technol.* **2020**, *104*, 103520. [[CrossRef](#)]
35. Systèmes, D. *Abaqus User Manual, Version 6.14*; Simulia Corp: Providence, RI, USA, 2014.
36. Qi, C.; Chen, Q.; Dong, X.; Zhang, Q.; Yaseen, Z.M. Pressure drops of fresh cemented paste backfills through coupled test loop experiments and machine learning techniques. *Powder Technol.* **2019**, *361*, 748–758. [[CrossRef](#)]

37. Golbraikh, A.; Tropsha, A. Beware of q^2 ! *J. Mol. Graph. Model.* **2002**, *20*, 269–276. [[CrossRef](#)] [[PubMed](#)]
38. Roy, P.P.; Roy, K. On Some Aspects of Variable Selection for Partial Least Squares Regression Models. *QSAR Comb. Sci.* **2008**, *27*, 302–313. [[CrossRef](#)]

Disclaimer/Publisher's Note: The statements, opinions and data contained in all publications are solely those of the individual author(s) and contributor(s) and not of MDPI and/or the editor(s). MDPI and/or the editor(s) disclaim responsibility for any injury to people or property resulting from any ideas, methods, instructions or products referred to in the content.